of cardiovascular function, the central role of NO in the modulation of the pulmonary vasculature needs to be addressed. Therefore, our first aim in the present study was to elucidate the role of NO in the central modulation of pulmonary vascular tone under normoxic conditions and after the development of chronic hypoxia-induced pulmonary hypertension. Nitric oxide is thought to have an important role in modulating the hypoxic pulmonary vasoconstriction (HPV) in response to acute hypoxic challenges.[26] However, there are conflicting reports as to whether the HPV response is accentuated or attenuated by pulmonary hypertension.[6,27] Therefore, a second aim of the present study was to assess the acute HPV before and after chronic hypoxia and to determine whether central NO has a role in modulating this response.

METHODS

Animals

Experiments were conducted on 23 male Sprague-Dawley rats (8 weeks old; bodyweight approximately 200–280 g). Rats were divided into four groups, as follows: (i) group 1, normoxia (N) + L-NAME; (ii) group 2, chronic hypoxia (CH) + L-NAME; (iii) group 3, N + 3-morpholino-sydnonimine hydrochloride (SIN-1); and (iv) group 4, CH + SIN-1. The CH rats were housed in a hypoxic chamber (12.0 ± 0.1% O_2) continuously for 2 weeks, except for a 10 min interval each day when the chamber was cleaned. The N rats were housed in similar housing, except that N rats breathed room air. The hypoxic gas mixture was delivered to the hypoxic chamber (30 L capacity) at a flow rate of approximately 8 L/min. All rats were on a 12 h light/dark cycle at 25 ± 1°C and were provided with food and water *ad libitum*. All experiments were approved by the local Animal Ethics Committee and conducted in accordance with the guidelines of the Physiological Society of Japan (http://www.soc.nii.ac.jp/psj/).

Anaesthesia and surgery

Rats were initially anaesthetized with pentobarbitone sodium (45 mg/kg, i.p.) and supplementary doses of anaesthetic were administered periodically throughout the experimental protocol (15–30 mg/kg per h, i.p.) so as to maintain a constant surgical level of anaesthesia (assessed by using the limb withdrawal reflex test). Rectal temperature was maintained at 38°C using a rectal thermistor coupled to a thermostatically controlled heating pad.

Using a stereotaxic frame, the tip of a 27 gauge stainless steel cannula was positioned in the right lateral cerebral ventricle based on the coordinates of Paxinos and Watson[28] (0.8 mm posterior to the bregma, 1.5 mm lateral to the midline and 5.0 mm ventral to the skull surface). The distal end of the cannula was connected to a 0.5 mL syringe for subsequent drug administration. Correct positioning of the intracerebroventricular (i.c.v.) catheter was confirmed after each experiment by staining with Evans blue dye (10 μL).

The trachea was cannulated and the lungs ventilated with a rodent ventilator (SN-480-7; Shinano, Tokyo, Japan). The inspirate gas was enriched with O_2 (approximately 50% O_2) and the ventilator settings were adjusted (tidal volume (V_T) approximately 3.5 mL; frequency approximately 80 /min) to maintain arterial P_{CO_2} normocapnic. The femoral artery and vein were cannulated for the measurement of systemic arterial blood pressure and drug administration, respectively. The arterial line contained heparinized saline (50 U/mL). A right thoracotomy was made between the second and third ribs and the conus of the right ventricle was exposed. A 23 gauge needle was used to pierce the ventricle wall and then the gel-filled sensing catheter of a telemetric transmitter (model TA11PA-C40; Data Sciences, St Paul, MN, USA) was inserted anteriorly into the right ventricle and advanced into the pulmonary artery. The catheter was fixed in position with a 7.0 Prolene suture to the pericardium. The aorta was blunt dissected free from the pulmonary artery and a transonic perivascular flowprobe (model 2RB; Transonic Systems, Ithaca, NY, USA) was positioned around the ascending aorta for the continuous measurement of cardiac output.

Drugs

Artificial cerebrospinal fluid (aCSF) was used as the vehicle for administering the NOS inhibitor L-NAME and the slow-releasing NO donor, 3-[4-morpholinyl]-sydnonimine-hydrochloride (SIN-1). The aCSF (pH 7.36–7.43) was comprised of 150 mmol/L NaCl, 3.0 mmol/L KCl, 0.8 mmol/L $MgCl_2$, 1.4 mmol/L $CaCl_2$ and 1.0 mmol/L Na phosphate. Intracerebroventricular injections were given as a 10 μL bolus over 30 s. Intravenous (i.v.) injections were administered as a 0.2 mL bolus over 15 s, followed by a 0.1 mL saline flush.

Measurement of right ventricular weight

Immediately following the experiment, rats were killed by anaesthetic overdose, the heart was excised, the atria were removed and the right ventricle wall was separated from the left ventricle, including the septum. Tissues were blotted and weighed. Right and left ventricular weights were expressed as the ratio of the right ventricle to the left ventricular + septum weight ($W_{RV}/W_{LV+septum}$; Fulton's ratio).

Experimental protocols

Once all variables had stabilized after surgery (approximately 20 min), baseline values were recorded for 10 min in response to the i.c.v. administration of aCSF (10 μL). The inspirate was then switched to hypoxia (10% O_2 balanced by N_2) for 4 min. Upon recovery from acute hypoxia, rats received a bolus i.c.v. injection of either L-NAME (150 μg; groups 1 and 2) or SIN-1 (100 μg; groups 3 and 4). After 5 (L-NAME) or 10 min (SIN-1), the acute hypoxic test was repeated. After a further 10 min, once variables had recovered to prehypoxic values, rats (groups 1 and 2 only) received a bolus i.v. injection of L-NAME (50 mg/kg) and acute hypoxia was tested 10 min later.

Data acquisition and analysis

Pulmonary arterial pressure was measured using telemetry. The signal from the implanted transmitter (model TA11PA-C20; Data Sciences) was calibrated in reference to an input from an ambient-pressure monitor (C11PR; Data Sciences) and subsequently relayed to a personal computer. Cardiac output (CO) was measured continuously from the ascending aorta using a Transonic small animal blood flowmeter (model T206; Transonic Systems) with a flowprobe (model 2RB). Arterial blood pressure (ABP) was measured continuously with a Deltran pressure transducer (Utah Medical Products, Midvale, UT, USA) and the signal was relayed to a Powerlab bridge amplifier (ML117; ADInstruments, Tokyo, Japan).

The signals for ABP, CO and PAP were relayed from their respective units and sampled continuously at 200 Hz with an eight-channel MacLab/8s interface hardware system (ADInstruments) and recorded on a Macintosh Power Book G4 using Chart (v. 5.0.1; ADInstruments). Heart rate (HR) was derived from the arterial systolic peaks. Cardiac output was normalized (off-line) to 100 g bodyweight. Total systemic vascular resistance (SVR) and total pulmonary vascular resistance (PVR) were calculated by dividing mean ABP (MABP) and mean PAP (MPAP) by the normalized CO. A 10 block of data was analysed −60, −30 s and immediately before (time '0') acute hypoxic exposure and then after 20, 40, 60, 90, 120, 180 and 240 s of exposure to 10% O_2. Normoxic data for individual rats in each group were averaged from values acquired at −60, −30 s and at time 0. An arterial blood sample (0.1 mL) was extracted 5 min after the completion of surgery for analysis of arterial P_{CO_2} using an ABL 605 blood gas analyser (Radiometer, Copenhagen, Denmark). An additional 0.1 mL was extracted to measure haematocrit.

Statistical analysis

All statistical analyses were conducted using Statview (v. 5.01; SAS Institute, Cary, NC, USA). All results are presented as the mean±SEM. Two-way ANOVA (repeated measures) was used to test significance for: (i) changes in each variable in response to 4 min of acute hypoxia; and (ii) whether the hypoxic response was altered by drug administration (i.c.v. or i.v.).

One-way ANOVA (factorial) was used to test for differences in baseline values for normoxic and chronic hypoxic groups of rats. Where statistical significance was reached, post hoc analyses were incorporated using the paired or unpaired *t*-test with Dunnet's correction for multiple comparisons. $P \leq 0.05$ was predetermined as the level of significance for all statistical analyses.

RESULTS

Chronic hypoxia induced pulmonary hypertension (Table 1), as evidenced by the observation that the MPAP and PVR of CH rats ($n = 11$) was 50 and 34% higher, respectively, than that of normoxic (N) rats ($n = 12$; $P < 0.01$). Consequently, CH rats developed right ventricular hypertrophy (ΔRV/LV + Sep ratio of 0.23). Chronic hypoxia did not significantly change MABP or CO, but it did cause a significant reduction in HR (ΔHR 37 b.p.m.; $P < 0.01$), suggesting that the development of right ventricular hypertrophy resulted in an increase in stroke volume. An increase in haematocrit (ΔHct 18%; $P < 0.001$) also occurred in CH.

Responses to acute hypoxia

In N rats, acute exposure to 10% O_2 provoked an increase in MPAP, after a latency of 65–88 s, which reached a plateau after approximately 180 s (Fig. 1a). By 4 min, MPAP had increased significantly by 31 ± 5%, in spite of a small, albeit not significant, decline in both HR (6 ± 1%) and CO (16 ± 6%), reflecting substantial pulmonary vasoconstriction (67 ± 13% increase in PVR). Acute hypoxia also provoked a 56 ± 2% decrease in MABP by the end of the 4th min, which was primarily due to systemic vasodilatation (46 ± 3% decrease in SVR; Fig. 1a). Although CH slightly altered baseline values (detailed above), the magnitude of the response to 4 min hypoxia for MABP, HR, CO and SVR was essentially the same for the CH and N groups of rats (Fig. 1a,b). However, the potent pulmonary vasoconstriction seen in N rats was abolished in CH rats. Consequently, exposure to 10% O_2 did not cause a significant increase in MPAP or PVR in CH rats.

Administration of L-NAME

The maximum cardiovascular responses following a single i.c.v injection of L-NAME are given in Table 2. In N rats, L-NAME caused a small (<3% increase) but consistent increase in PVR ($P < 0.05$), although MPAP was not significantly affected. In addition, L-NAME caused a maximal 15 ± 4% increase in MABP after 35 ± 8 s, which was solely attributed to systemic vasoconstriction (16 ± 4% increase in SVR). All other variables were unaltered. The PVR, MABP and SVR responses were brief, returning to pre-L-NAME values within 4.5 min. Consequently, because acute hypoxia was tested 5 min after L-NAME injection, the prehypoxia baseline data were similar before and after L-NAME treatment. Furthermore, the magnitude of the cardiovascular responses to L-NAME for CH rats was statistically similar to that of N rats (Table 2). The i.c.v. administration of L-NAME did

Table 1 Baseline cardiovascular variables in rats exposed to normoxic or chronic hypoxia

	N rats	CH rats
MPAP (mmHg)	20.2 ± 1.1	30.4 ± 1.2**
MABP (mmHg)	106 ± 6	118 ± 4
CO (mL/min/100 g)	11.17 ± 0.75	12.32 ± 0.53
HR (b.p.m.)	416 ± 8	379 ± 11*
SVR (mmHg/mL per min per 100 g)	9.73 ± 0.64	9.72 ± 0.53
PVR (mmHg/mL per min per 100 g)	1.88 ± 0.14	2.52 ± 0.15*
RV/LV + Septum	0.31 ± 0.01	0.55 ± 0.02**
Haematocrit (%)	47 ± 1	65 ± 1**

Data are the mean±SEM. *$P < 0.01$, **$P < 0.001$ compared with normoxia values.

N, normoxic rats (groups 1 and 3; $n = 12$); CH, chronic-hypoxic rats (12% O_2 for 2 weeks; groups 2 and 4; $n = 11$); MPAP, mean pulmonary arterial pressure; MABP, mean arterial blood pressure; CO, cardiac output; HR, heart rate; SVR, systemic vascular resistance; PVR, pulmonary vascular resistance; RV, right ventricle; LV, left ventricle.

Table 2 Maximum responses to intracerebroventricular N^G-nitro-L-arginine methyl ester (150 μg in 10 μL) in normoxic rats ($n = 7$) and chronic hypoxic rats ($n = 5$)

	Normoxia		Chronic hypoxia	
	Pre-L-NAME	Max L-NAME	Pre-L-NAME	Max L-NAME
MPAP (mmHg)	18.6 ± 0.6	19.0 ± 0.6	30.4 ± 1.6	31.1 ± 1.9
MABP (mmHg)	102 ± 10	116 ± 8**	110 ± 5	120 ± 5*
CO (mL/min per 100 g)	10.12 ± 1.10	10.09 ± 1.13	12.24 ± 1.07	11.98 ± 1.00
HR (b.p.m.)	413 ± 10	416 ± 9	373 ± 13	376 ± 14
SVR (mmHg/mL per min per 100 g)	10.79 ± 1.85	12.39 ± 2.05**	9.14 ± 0.55	10.19 ± 0.66*
PVR (mmHg/mL per min per 100 g)	1.94 ± 0.20	2.00 ± 0.21*	2.53 ± 0.18	2.64 ± 0.21*

Data are the mean±SEM. *$P < 0.05$, **$P < 0.01$ compared with pre-N^G-nitro-L-arginine methyl ester (L-NAME).

MPAP, mean pulmonary arterial pressure; MABP, mean arterial blood pressure; CO, cardiac output; HR, heart rate; SVR, systemic vascular resistance; PVR, pulmonary vascular resistance.

not alter the acute hypoxic response for any of the variables recorded in either N or CH rats (Fig. 1a,b).

Cardiovascular responses to the i.v. administration of L-NAME (50 mg/kg, i.v.) were also recorded. In N rats, a bolus i.v. dose of L-NAME provoked robust systemic vasoconstriction (123 ± 20% increase in SVR; $P < 0.001$), as well as, to a lesser extent, pulmonary vasoconstriction (80 ± 10% increase in PVR; $P < 0.01$). The baroreflex decrease in HR and CO (NS; see baseline data in Fig. 1a,b) meant that the changes in vascular resistance were accompanied by smaller, but still significant, increases in MABP (42 ± 18% increase in MABP; $P < 0.001$) and MPAP (13 ± 9% increase in MPAP; NS) in N rats. After 2 weeks of chronic hypoxia, L-NAME (i.v.) had a similar effect on the systemic vasculature and caused a similar depression of HR (NS) and CO ($P < 0.001$), but it had a more pronounced effect on the pulmonary vasculature (24 ± 5% increase in MPAP (NS); 116 ± 18% increase in PVR ($P < 0.01$)).

Treatment of N rats with L-NAME (i.v.) exacerbated the reduction in MABP and SVR in response to acute hypoxia and accentuated the increase in MPAP and PVR (Fig. 1a,b). Despite a depression in baseline values for CO and HR, i.v. administration of L-NAME did not change the transient responses to hypoxia. In CH rats, the transient MABP and SVR responses to acute hypoxia were elevated by L-NAME (i.v.). In addition, L-NAME restored the potent MPAP (and PVR) response to acute hypoxia (observed in N rats), which had been absent prior to L-NAME treatment (Fig. 1a,b).

Administration of SIN-1

Following a single bolus i.c.v. injection of SIN-1 (100 μg) in N rats, baseline MPAP and PVR were not significantly altered. However, MABP declined slowly before stabilizing 38 ± 7% below the pre-SIN-1 baseline (Table 3). Preliminary studies

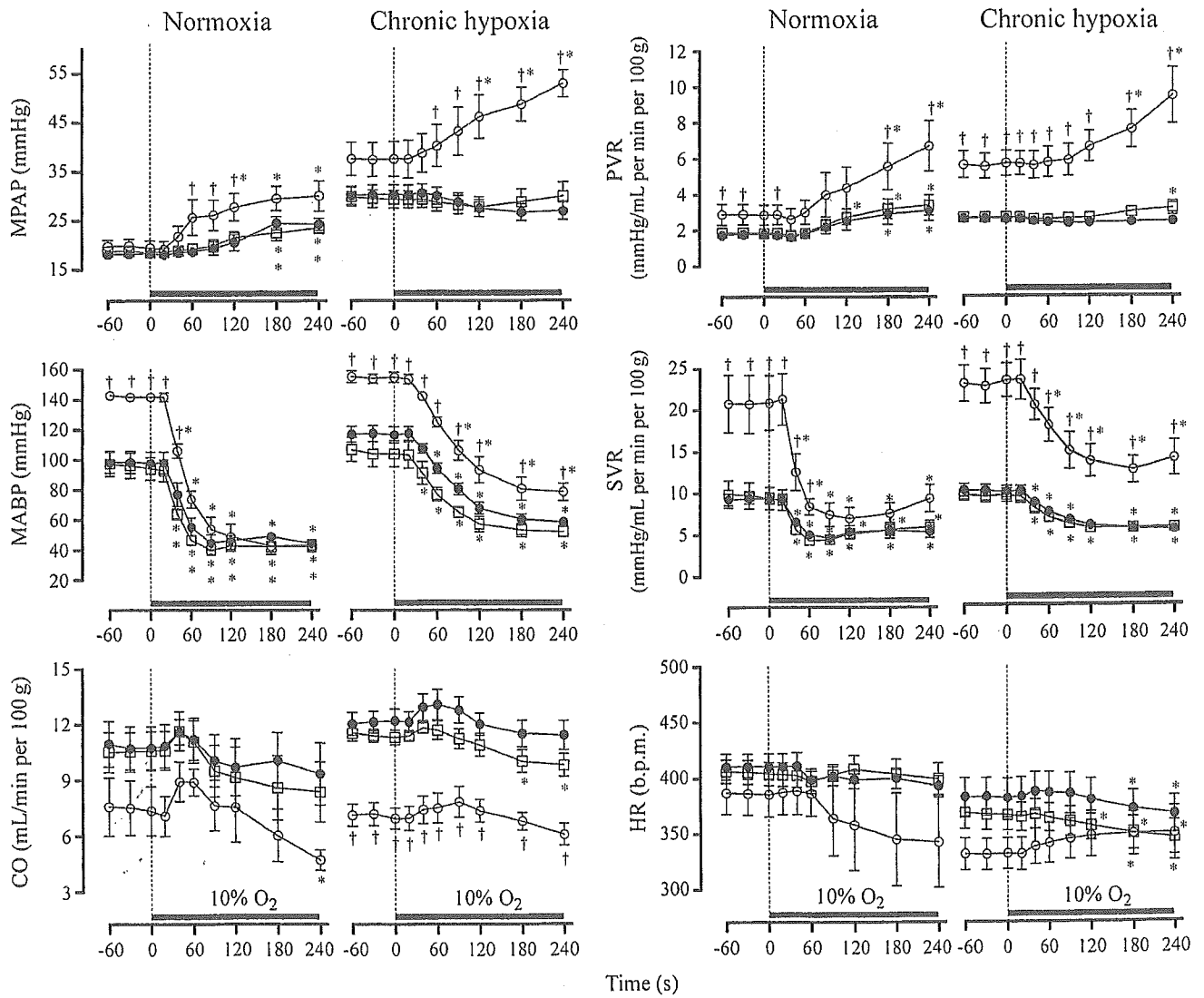

Fig. 1 Mean pulmonary arterial pressure (MPAP), mean arterial blood pressure (MABP), cardiac output (CO), pulmonary vascular resistance (PVR), systemic vascular resistance (SVR) and heart rate (HR) responses to acute hypoxia (10% O_2 for 4 min) in normoxic (N) rats ($n = 7$) and chronic hypoxic (CH) rats ($n = 5$), before (●) and after the administration of N^G-nitro-L-arginine methyl ester (L-NAME; □, 150 μg in 10 μL, i.c.v.; ◇, 50 mg/kg, i.v.). $^*P < 0.05$ compared with pre-acute hypoxia values; $^\dagger P < 0.05$ compared with L-NAME values.

showed that once cardiovascular variables stabilized following the initial response to SIN-1, variables did not change for at least another 20 min. The fall in MABP was primarily attributed to vasodilatation (29 ± 7% decrease in SVR; $P < 0.05$). In CH rats, SIN-1 (i.c.v.) did not alter PVR, but it did decrease MPAP by 21 ± 3% ($P < 0.01$) owing to a 22 ± 5% decrease in CO ($P < 0.05$). Syndnonimine-1 provoked a larger decrease in CO in CH rats (22 ± 5% decrease; $P < 0.05$), so that the fall in MABP was also greater in CH rats (46 ± 3% decrease), because the decline in SVR was similar for N rats and CH rats (27 ± 7 and 29% decrease in SVR, respectively).

In N rats, the CO response to acute hypoxia was depressed by SIN-1 so that, even though the MPAP response appeared to be unchanged (Fig. 2a), the PVR response to hypoxia was accentuated by SIN-1 (64 ± 24 and 127 ± 26% increase, respectively; Fig. 2b). Syndnonimine-1 reduced the magnitude of the MABP and SVR responses to hypoxia, although the absolute MABP (and SVR) values during hypoxia before and after SIN-1 were similar. In addition, SIN-1 abolished the small hypoxia-induced decline in HR observed prior to SIN-1 administration.

In CH rats, SIN-1 restored the pulmonary vasoconstriction in response to acute hypoxia. This was evident by a 33 ± 5% increase in MPAP (cf. a 3% increase for control) and a 90 ± 11% increase in PVR (cf. a 20% increase for control). The effect of SIN-1 on the MABP, SVR, CO and HR responses to acute hypoxia were similar for N and CH rats (Fig. 2a,b).

DISCUSSION

To date, this is the first study to investigate the central role of NO in: (i) modulating MPAP in the normal and hypertensive state; and (ii) acute HPV. The primary findings of the present study show that, in both N and CH rats, the acute central inhibition of NOS does not appear to modulate baseline MPAP or pulmonary vascular

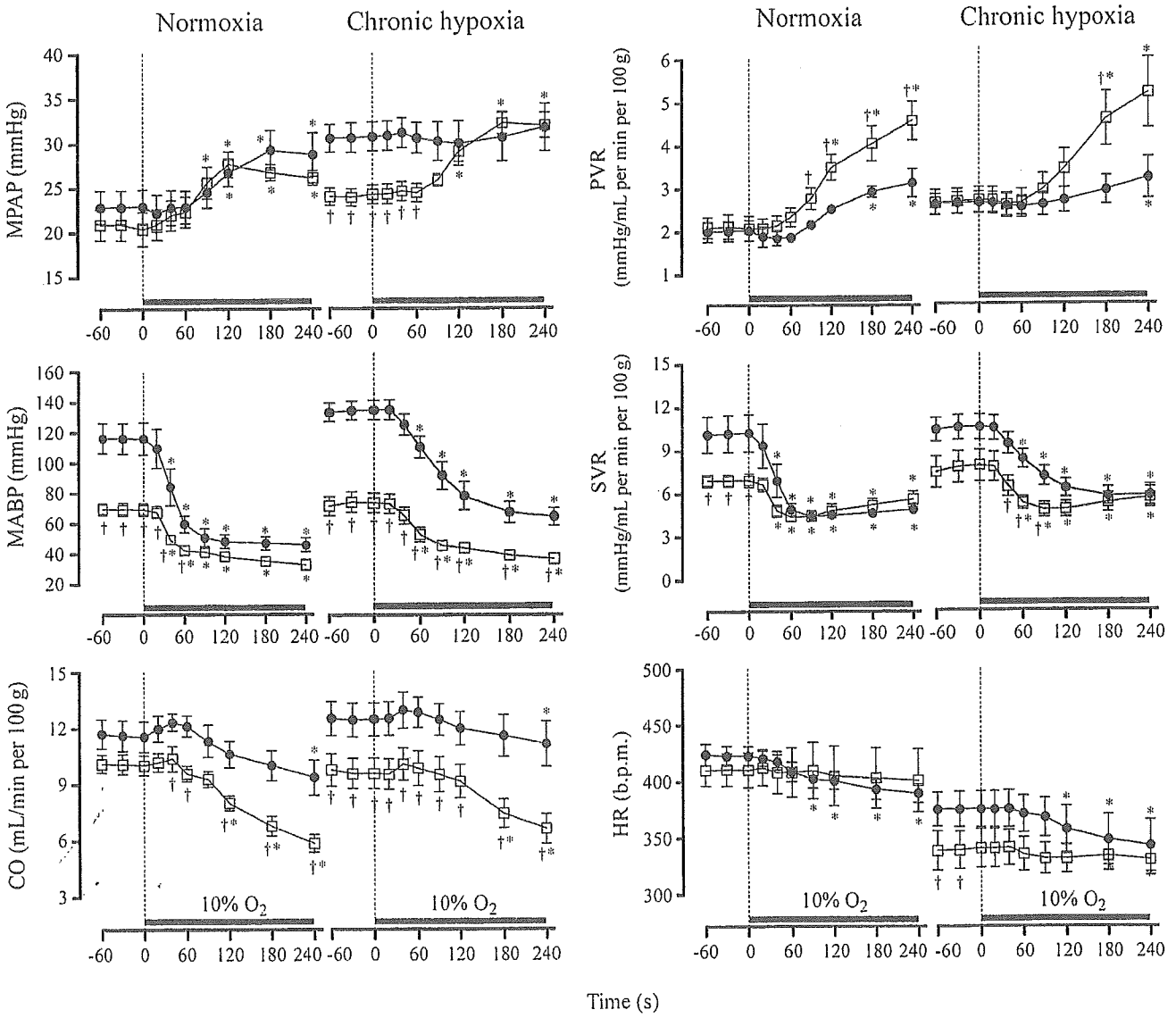

Fig. 2 Effect of i.c.v. syndnonimine-1 (SIN-1) on mean pulmonary arterial pressure (MPAP), mean arterial blood pressure (MABP), cardiac output (CO), pulmonary vascular resistance (PVR), systemic vascular resistance (SVR) and heart rate (HR) responses to acute hypoxia (10% O_2 for 4 min) in normoxic (N) rats ($n = 5$) and chronic hypoxic (CH) rats ($n = 6$). (●), control (artificial cerebrospinal fluid); (□), SIN-1 (100 μg in 10 μL). *$P < 0.05$ compared with pre-acute hypoxia values; †$P < 0.05$ compared with SIN-1-values.

Table 3 Steady state responses to intracerebroventricular syndnonimine-1 (100 μg in 10 μL) in normoxic rats ($n = 5$) and chronic-hypoxic rats ($n = 6$)

	Normoxia		Chronic hypoxia	
	Control	SIN-1	SIN-1	Control
MPAP (mmHg)	22.9 ± 1.7	20.8 ± 1.8	30.6 ± 1.6	24.1 ± 1.0*
MABP (mmHg)	116 ± 10	69 ± 4*	122 ± 6	67 ± 6**
CO (mL/min per 100 g)	11.64 ± 0.81	10.08 ± 0.51	12.46 ± 0.89	9.63 ± 0.81*
HR (b.p.m.)	423 ± 9	410 ± 15	375 ± 16	339 ± 17**
SVR (mmHg/mL per min per 100 g)	10.20 ± 1.28	6.93 ± 0.42*	10.07 ± 0.82	7.36 ± 1.06*
PVR (mmHg/mL per min per 100 g)	2.02 ± 0.23	2.10 ± 0.27	2.54 ± 0.24	2.58 ± 0.28

Data are the mean±SEM. *$P < 0.05$, **$P < 0.01$ compared with control values.

SIN-1, syndnonimine-1; MPAP, mean pulmonary arterial pressure; MABP, mean arterial blood pressure; CO, cardiac output; HR, heart rate; SVR, systemic vascular resistance; PVR, pulmonary vascular resistance.

reactivity to acute hypoxia. However, exogenous NO reduces baseline MPAP in CH rats, primarily by reducing CO, and enhances the HPV.

We demonstrated that exposure to 12% O_2 for 2 weeks induced pulmonary arterial hypertension, which concurs with numerous reports in the literature regarding the effects of CH on the pulmonary vasculature.[6,29,30] Compared with the pulmonary vasculature, the systemic vasculature seems to be less affected by CH. We did not observe any difference in MABP between N and CH rats, which is similar to some reports.[30,31] In contrast, Huang *et al.*[6] did note an increase in MABP after 2 weeks of CH, although they described the increase in MABP as mild compared with the increase in MPAP.

The mechanisms responsible for the development of pulmonary hypertension remain poorly understood. Although a reduction in the local release of NO from the pulmonary endothelium has been implicated,[5,8,32] Hampl *et al.*[30] reported that chronic inhibition of NOS did not increase MPAP, indicating that factors other than, or in addition to, a decrease in pulmonary NOS activity were responsible for the development of pulmonary hypertension. Furthermore, Weissmann *et al.*[27] investigated the role of pulmonary NO in the acute HPV response and concluded that attenuation of the acute HPV by chronic hypoxia preceded the development of pulmonary hypertension and was independent of the pulmonary endothelial NO system. Therefore, we hypothesized that disruption of the central NO pathways may contribute, at least in part, to the pathogenesis of pulmonary hypertension during chronic hypoxia.

Our results indicate that, using L-NAME, central NO has a minimal role, if any, in modulating tonic pulmonary vascular tone in the normal and hypertensive state. However, we cannot rule out the possibility that the dose of L-NAME selected in the present study did not completely inhibit NOS within the cardiovascular control centres. Preliminary experiments indicated that when L-NAME is injected i.v., doses above 150 μg had small direct systemic effects (similar preliminary experiments were conducted to determine the dose of SIN-1 with which to inject i.c.v. that did not directly alter pulmonary vasculature when injected i.v.). Therefore, because L-NAME can cross the blood–brain barrier,[33] we avoided higher doses of L-NAME that could have potentially directly modulated pulmonary vascular tone. Furthermore, a study by Nurminen *et al.*[34] reported that 30 μg L-NAME, i.c.v., provoked a significant increase in ABP that lasted for 10 min. Therefore, we were confident that a dose of 150 μg L-NAME would induce sufficient central NOS inhibition.

Although we found that L-NAME did not alter the acute HPV, we cannot exclude the possibility that the central actions of L-NAME had fully subsided before testing acute hypoxia. However, preliminary experiments (data not shown) indicated that, even when L-NAME was administered immediately before the acute hypoxic test, the cardiovascular responses to acute hypoxia were not different to the responses prior to L-NAME. Alternatively, acute hypoxia is known to be a powerful activator of sympathetic nerve activity.[35] Because it has been well documented that the central administration of L-NAME increases sympathetic activity,[36,37] it may be possible that, in the present study, L-NAME did not alter the HVR because sympathetic activity was already elevated by the acute hypoxic stimulus.

Although central L-NAME did not alter pulmonary vasculature tone, the intravenous administration of L-NAME did cause a small increase in PVR in N rats, which was accentuated after chronic hypoxia. Furthermore, the acute HVR was accentuated by L-NAME (i.v.) in both N and CH rats. Several studies have indicated that local endothelial NO has a limited role, if any, in the tonic modulation of MPAP,[6,38] although Huang *et al.*[6] indicated that local NO: (i) was more important in modulating pulmonary vasculature after chronic hypoxia; and (ii) was essential for maintaining low pulmonary resistance during acute hypoxia.

In comparison, the magnitude of the systemic vasoconstrictive response to L-NAME (i.v.) was substantially larger than that of the pulmonary vasculature. In agreement, several studies have indicated that local inhibition of NOS has an insignificant effect on tonic modulation of the pulmonary vasculature, but it is critical in modulating the systemic vasculature.[6,30,38]

It has been well documented that central inhibition of NO increases MABP[34,39,40] by increasing sympathetic nerve activity.[36,37] We also reported that i.c.v. L-NAME provoked a significant increase in MABP, although one of the limitations of the present study is that we did not measure sympathetic activity. However, we found that the provoked increase in MABP by i.c.v. L-NAME in the normoxic rat was not accompanied by a baroreflex decrease in HR, which occurs when L-NAME is injected intravenously. Nurminen *et al.*[34] also reported that i.c.v. L-NAME caused a paradoxical increase in HR and, thus, concluded that the increase in HR was indirect evidence that L-NAME provoked an increase in sympathetic activity.

With regards to the pulmonary vasculature, an increase in sympathetic activity can cause either vasoconstriction (α-adrenoreceptor mediated) or vasodilation (β-adrenoreceptor mediated), depending on the initial pulmonary vascular tone.[41,42] Therefore, assuming that i.c.v. L-NAME did increase pulmonary sympathetic activity, it is possible that we were unable to detect any change

in MPAP because of the potential opposing effects of α- and β-adrenoceptor activation within the pulmonary vasculature.

In the present study, as well as in other studies, the central administration of NO donors has been shown to reduce MABP.[25,43] Nurminen and Vapaatalo[44] also showed that certain NO-releasing substances, such as nitroprusside, reduced MABP, although they also mentioned that the central administration of SIN-1 (approximately 600 μg/kg) increased MABP.

At high doses, SIN-1 can cogenerate NO and superoxide anions.[45,46] Furthermore, an increase in the central generation of superoxide anions has been reported to increase sympathetic activity and, consequently, ABP.[47] Therefore, the increase in MABP in the study of Nurminen and Vapaatalo[44] may be attributed to the formation of superoxide anions. At low doses, the superoxide-associated effects of SIN-1 are significantly outweighed by the actions of NO.[45] Therefore, because the present study used a comparatively low dose of SIN-1 (100 μg), we interpret the decrease in MABP to indicate that, at this dose, SIN-1 was acting solely as an NO donor.

The decrease in MABP following the central administration of exogenous NO has been attributed to a decrease in sympathetic activity.[40,48] To date, the present study is the first to investigate the effects of a central NO donor on MPAP. The important finding of the present study is that exogenous NO did not directly alter baseline pulmonary vascular tone (i.e. PVR was not altered), but it did enhance (in N rats) or restore (in CH rats) the acute HPV response. These results support the idea that central NO has little influence on the tonic modulation of pulmonary vascular tone, although it enhances the acute HPV.

Although we cannot confirm the underlying mechanisms responsible for these observations, it is possible that SIN-1 did reduce sympathetic activity in the rats in the present study, subsequently enhancing the HPV. Shirai *et al.*[49] demonstrated that β-adrenoceptor blockade had only a minor effect on baseline pulmonary vascular tone in normoxia, but it significantly accentuated the acute HPV (α-adrenoceptor blockade had no effect on the magnitude of the HPV). This observation may explain the reason as to why central SIN-1 did not affect baseline PVR but accentuated the HPV in the present study. Although PVR was not affected, central SIN-1 did reduce MPAP in the present study (significantly in CH rats), solely due to a reduction in CO. This, too, may be due to a reduction in β-adrenoceptor activity, because β-adrenoceptor attenuation has been reported to significantly reduce CO.[50,51]

The mechanism(s) responsible for the attenuation of the HPV after chronic hypoxia remain poorly understood. However, it is possible to speculate that β-adrenoceptor upregulation may be one contributing factor because previous studies have shown that chronic hypoxia significantly increases β-adrenoceptor numbers within the lung.[52,53] Changes in β-adrenoceptor availability during chronic hypoxia could potentially limit the development of pulmonary hypertension and, therefore, be physiologically beneficial; an important area that warrants further research.

In summary, we have shown that central NO has a limited role in modulating tonic MPAP in the normal and hypertensive states. However, exogenous NO enhanced the acute HPV, although central NO inhibition had no effect on the acute HPV. Whether central NO acts to inhibit β-adrenoceptor-mediated vasodilation of the acute HPV is another area that warrants further investigation. The present study used an anaesthetized preparation to investigate the modulation of MPAP in normoxia and after chronic hypoxia. We did not, however, address any potential changes in the control of MPAP during the development of pulmonary hypertension. Hampl and Herget[38] indicated that, during the development of pulmonary hypertension, NO was essential in preventing pulmonary hypertension in the early stages, but became insignificant in the latter stages owing to endothelial dysfunction. Therefore, we will subsequently develop a conscious, chronically cannulated rat model to monitor the development of pulmonary hypertension during the chronic central inhibition/infusion of NO.

ACKNOWLEDGEMENT

The authors are very grateful for the aid and support provided by the Japan Society for the Promotion of Science (JSPS).

REFERENCES

1. Archer S, Rich S. Primary pulmonary hypertension: A vascular biology and translational research 'work in progress'. *Circulation* 2000; **102**: 2781–91.
2. Mandegar M, Yuan JX. Role of K^+ channels in pulmonary hypertension. *Vasc. Pharmacol.* 2002; **38**: 25–33.
3. Barbera JA, Peinado VI, Santos S. Pulmonary hypertension in COPD: Old and new concepts. *Monaldi Arch. Chest Dis.* 2000; **55**: 445–9.
4. Voelkel NF, Tuder RM. Hypoxia-induced pulmonary vascular remodeling: A model for what human disease? *J. Clin. Invest.* 2000; **106**: 733–8.
5. Fike CD, Kaplowitz MR, Thomas CJ, Nelin LD. Chronic hypoxia decreases nitric oxide production and endothelial nitric oxide synthase in newborn pig lungs. *Am. J. Physiol.* 1998; **274**: L517–26.
6. Huang KL, Wu CP, Kang BH, Lin YC. Chronic hypoxia attenuates nitric oxide-dependent hemodynamic responses to acute hypoxia. *J. Biomed. Sci.* 2002; **9**: 206–12.
7. Cornwell TL, Arnold E, Boerth NJ, Lincoln TM. Inhibition of smooth muscle cell growth by nitric oxide and activation of cAMP-dependent protein kinase by cGMP. *Am. J. Physiol.* 1994; **267**: C1405–13.
8. Le Cras TD, McMurtry IF. Nitric oxide production in the hypoxic lung. *Am. J. Physiol. Lung Cell. Mol. Physiol.* 2001; **280**: L575–82.
9. Sato J, Nair K, Hiddinga J *et al.* eNOS gene transfer to vascular smooth muscle cells inhibits cell proliferation via upregulation of p27 and p21 and not apoptosis. *Cardiovasc. Res.* 2000; **47**: 697–706.
10. Palmer RM, Rees DD, Ashton DS, Moncada S. L-Arginine is the physiological precursor for the formation of nitric oxide in endothelium-dependent relaxation. *Biochem. Biophys. Res. Commun.* 1988; **153**: 1251–6.
11. Fagan KA, Fouty BW, Tyler RC *et al.* The pulmonary circulation of homozygous or heterozygous eNOS-null mice is hyperresponsive to mild hypoxia. *J. Clin. Invest.* 1999; **103**: 291–9.
12. Steudel W, Ichinose F, Huang PL *et al.* Pulmonary vasoconstriction and hypertension in mice with targeted disruption of the endothelial nitric oxide synthase (NOS 3) gene. *Circ. Res.* 1997; **81**: 34–41.
13. Steudel W, Scherrer-Crosbie M, Bloch KD *et al.* Sustained pulmonary hypertension and right ventricular hypertrophy after chronic hypoxia in mice with congenital deficiency of nitric oxide synthase 3. *J. Clin. Invest.* 1998; **101**: 2468–77.
14. Ozaki M, Kawashima S, Yamashita T *et al.* Reduced hypoxic pulmonary vascular remodeling by nitric oxide from the endothelium. *Hypertension* 2001; **37**: 322–7.
15. Sato K, Rodman DM, McMurtry IF. Hypoxia inhibits increased ET_B receptor-mediated NO synthesis in hypertensive rat lungs. *Am. J. Physiol.* 1999; **276**: L571–81.
16. Xue C, Rengasamy A, Le Cras TD, Koberna PA, Dailey GC, Johns RA. Distribution of NOS in normoxic vs. Hypoxic rat lung:

Upregulation of NOS by chronic hypoxia. *Am. J. Physiol.* 1994; **267**: L667–78.
17. Shirai M, Pearson JT, Shimouchi A *et al.* Changes in functional and histological distributions of nitric oxide synthase caused by chronic hypoxia in rat small pulmonary arteries. *Br. J. Pharmacol.* 2003; **139**: 899–910.
18. Le Cras TD, Xue C, Rengasamy A, Johns RA. Chronic hypoxia upregulates endothelial and inducible NO synthase gene and protein expression in rat lung. *Am. J. Physiol.* 1996; **270**: L164–70.
19. Matsumura K, Tsuchihashi T, Kagiyama S, Abe I, Fujishima M. Role of nitric oxide in the nucleus of the solitary tract of rats. *Brain Res.* 1998; **798**: 232–8.
20. Zanzinger J, Czachurski J, Seller H. Inhibition of basal and reflex-mediated sympathetic activity in the RVLM by nitric oxide. *Am. J. Physiol.* 1995; **268**: R958–62.
21. Ohta A, Takagi H, Matsui T, Hamai Y, Iida S, Esumi H. Localization of nitric oxide synthase-immunoreactive neurons in the solitary nucleus and ventrolateral medulla oblongata of the rat: Their relation to catecholaminergic neurons. *Neurosci. Lett.* 1993; **158**: 33–5.
22. Garthwaite J, Boulton CL. Nitric oxide signaling in the central nervous system. *Annu. Rev. Physiol.* 1995; **57**: 683–706.
23. Patel KP, Li YF, Hirooka Y. Role of nitric oxide in central sympathetic outflow. *Exp. Biol. Med.* 2001; **226**: 814–24.
24. Hironaga K, Hirooka Y, Matsuo I *et al.* Role of endogenous nitric oxide in the brain stem on the rapid adaptation of baroreflex. *Hypertension* 1998; **31**: 27–31.
25. Nishimura M, Takahashi H, Nanbu A, Sakamoto M, Yoshimura M. Cardiovascular regulation by L-arginine in the brain of rats: Role of the brain renin–angiotensin system and nitric oxide. *Am. J. Hypertens.* 1997; **10**: 389–96.
26. Clini E, Ambrosino N. Nitric oxide and pulmonary circulation. *Med. Sci. Monit.* 2002; **8**: RA178–82.
27. Weissmann N, Nollen M, Gerigk B *et al.* Downregulation of hypoxic vasoconstriction by chronic hypoxia in rabbits: Effects of nitric oxide. *Am. J. Physiol. Heart Circ. Physiol.* 2003; **284**: H931–8.
28. Paxinos G, Watson C. *The Brain in Stereotaxic Coordinates*, 4th edn. Academic Press, San Diego, CA. 1998.
29. Ao Q, Huang L, Zhu P, Xiong M, Wang D. Inhibition of expression of hypoxia-inducible factor-1alpha mRNA by nitric oxide in hypoxic pulmonary hypertension rats. *J. Huazhong Univ. Sci. Technol. Med. Sci.* 2004; **24**: 5–8.
30. Hampl V, Archer SL, Nelson DP, Weir EK. Chronic EDRF inhibition and hypoxia: Effects on pulmonary circulation and systemic blood pressure. *J. Appl. Physiol.* 1993; **75**: 1748–57.
31. Coney AM, Bishay M, Marshall JM. Influence of endogenous nitric oxide on sympathetic vasoconstriction in normoxia, acute and chronic systemic hypoxia in the rat. *J. Physiol.* 2004; **555**: 793–804.
32. Adnot S, Raffestin B, Eddahibi S, Braquet P, Chabrie PE. Loss of endothelium-dependent relaxant activity in the pulmonary circulation of rats exposed to chronic hypoxia. *J. Clin. Invest.* 1991; **87**: 155–62.
33. Bansinath M, Arbabha B, Turndorf H, Garg UC. Chronic administration of a nitric oxide synthase inhibitor *N*-nitro-L-arginine, and drug-induced increase in cerebellar cyclic GMP *in vivo*. *Neurochem. Res.* 1993; **18**: 1063–6.
34. Nurminen ML, Ylikorkala A, Vapaatalo H. Central inhibition of nitric oxide synthesis increases blood pressure and heart rate in anesthetized rats. *Methods Fundam. Exp. Clin. Pharmacol.* 1997; **19**: 35–41.
35. Fletcher EC. Invited review: Physiological consequences of intermittent hypoxia: Systemic blood pressure. *J. Appl. Physiol.* 2001; **90**: 1600–5.
36. Harada S, Tokunaga S, Momohara M *et al.* Inhibition of nitric oxide formation in the nucleus tractus solitarius increases renal sympathetic nerve activity in rabbits. *Circ. Res.* 1993; **72**: 511–16.
37. Zanzinger J, Czachurski J, Seller H. Nitric oxide in the ventrolateral medulla regulates sympathetic responses to systemic hypoxia in pigs. *Am. J. Physiol.* 1998; **275**: R33–9.
38. Hampl V, Herget J. Role of nitric oxide in the pathogenesis of chronic pulmonary hypertension. *Physiol. Rev.* 2000; **80**: 1337–72.
39. Choi KC, Jung M, Lee JU, Kim SW, Kim NH, Kang YJ. Attenuated central pressor response to nitric oxide synthesis inhibition in chronic renal failure rats. *Korean J. Intern. Med.* 1997; **12**: 58–61.
40. Togashi H, Sakuma I, Yoshioka M *et al.* A central nervous system action of nitric oxide in blood pressure regulation. *J. Pharmacol. Exp. Ther.* 1992; **262**: 343–7.
41. Shirai M, Shindo T, Shimouchi A, Ninomiya I. Diameter and flow velocity changes of feline small pulmonary vessels in response to sympathetic nerve stimulation. *Pflügers Arch.* 1994; **429**: 267–73.
42. Shirai M, Matsukawa K, Nishiura N, Kawaguchi AT, Ninomiya I. Changes in efferent pulmonary sympathetic nerve activity during systemic hypoxia in anesthetized cats. *Am. J. Physiol.* 1995; **269**: R1404–9.
43. Matsumura K, Abe I, Tsuchihashi T, Fujishima M. Central nitric oxide attenuates the baroreceptor reflex in conscious rabbits. *Am. J. Physiol.* 1998; **274**: R1142–9.
44. Nurminen ML, Vapaatalo H. Effect of intracerebroventricular and intravenous administration of nitric oxide donors on blood pressure and heart rate in anaesthetized rats. *Br. J. Pharmacol.* 1996; **119**: 1422–6.
45. Stopper H, Moller M, Bommel HM, Schmidt HH. Cytotoxic versus genotoxic effects of nitric oxide (NO). *Toxicol. Lett.* 1999; **106**: 59–67.
46. Megson IL, Webb DJ. Nitric oxide donor drugs: Current status and future trends. *Expert Opin. Investig. Drugs* 2002; **11**: 587–601.
47. Gao L, Wang W, Li YL *et al.* Superoxide mediates sympathoexcitation in heart failure: Roles of angiotensin II and NAD(P)H oxidase. *Circ. Res.* 2004; **95**: 937–44.
48. Shapoval LN, Sagach VF, Pobegailo LS. Nitric oxide influences ventrolateral medullary mechanisms of vasomotor control in the cat. *Neurosci. Lett.* 1991; **132**: 47–50.
49. Shirai M, Shindo T, Ninomiya I. β-Adrenergic mechanisms attenuated hypoxic pulmonary vasoconstriction during systemic hypoxia in cats. *Am. J. Physiol.* 1994; **266**: H1777–85.
50. Kontos HA, Lower RR. Role of beta-adrenergic receptors in the circulatory response to hypoxia. *Am. J. Physiol.* 1969; **217**: 756–63.
51. Chiong MA, Hatcher JD. The sympathoadrenergic system in the cardiovascular responsess to hypoxia in the dog. *Can. J. Physiol. Pharmacol.* 1972; **50**: 674–83.
52. Birnkrant DJ, Davis PB, Ernsberger P. Visualization of high- and low-affinity beta-adrenergic receptors in rat lung: Upregulation by chronic hypoxia. *Am. J. Physiol.* 1993; **265**: L389–94.
53. Winter RJ, Dickinson KE, Rudd RM, Sever PS. Tissue specific modulation of beta-adrenoceptor number in rats with chronic hypoxia with an attenuated response to down-regulation by salbutamol. *Clin. Sci.* 1986; **70**: 159–65.

Annual Report of Iwate Medical University
School of Liberal Arts and Sciences
No. 40 (2005), 1 - 7.

X-ray Spectra from a Characteristic X-ray Generator with a Molybdenum Tube

Eiichi Sato[a], Etsuro Tanaka[b], Hidezo Mori[c], Toshiaki Kawai[d], Takashi Inoue[e], Akira Ogawa[e], Kiyomi Takahashi[f], Shigehiro Sato[f] and Kazuyoshi Takayama[g]

(Received October 31, 2005)

Abstract

This generator consists of the following components: a constant high-voltage power supply, a filament power supply, a turbomolecular pump, and an x-ray tube. The x-ray tube is a demountable diode which is connected to the turbomolecular pump and consists of the following major devices: a molybdenum rod target, a tungsten hairpin cathode (filament), a focusing electrode, a polyethylene terephthalate x-ray window 0.25 mm in thickness, and a stainless-steel tube body. In the x-ray tube, the positive high voltage is applied to the anode (target) electrode, and the cathode is connected to the tube body (ground potential). In this experiment, the tube voltage applied was from 22 to 36 kV, and the tube current was regulated to within 100 μA by the filament temperature. The exposure time is controlled in order to obtain optimum x-ray intensity. The electron beams from the cathode are converged to the target by the focusing electrode, and x-rays are produced through the focusing electrode. Using a lithium fluoride curved crystal, clean K-series characteristic x-rays were observed without using a filter. However, bremsstrahlung x-rays were observed using a cadmium telluride detector.

Keywords: demountable x-ray tube, quasi-monochromatic x-rays, K-series characteristic x-rays, Sommerfeld's theory, curved crystal, cadmium telluride detector

1. Introduction

Most flash x-ray generators employ high-voltage condensers and cold-cathode x-ray tubes,[1-5] and the plasma x-ray source has been growing with increases in the electrostatic energy in the condenser. By

[a] Department of Physics, Iwate Medical University, 3-16-1 Honchodori, Morioka 020-0015, Japan
[b] Department of Nutritional Science, Faculty of Applied Bio-science, Tokyo University of Agriculture, 1-1-1 Sakuragaoka, Setagaya-ku 156-8502, Japan
[c] Department of Cardiac Physiology, National Cardiovascular Center Research Institute, 5-7-1 Fujishirodai, Suita, Osaka 565-8565, Japan
[d] Electron Tube Division #2, Hamamatsu Photonics K. K., 314-5 Shimokanzo, Iwata 438-0193, Japan
[e] Department of Neurosurgery, School of Medicine, Iwate Medical University, 19-1 Uchimaru, Morioka 020-8505, Japan
[f] Department of Microbiology, School of Medicine, Iwate Medical University, 19-1 Uchimaru, Morioka 020-8505, Japan
[g] Shock Wave Research Center, Institute of Fluid Science, Tohoku University, 2-1-1 Katahira, Sendai 980-8577, Japan

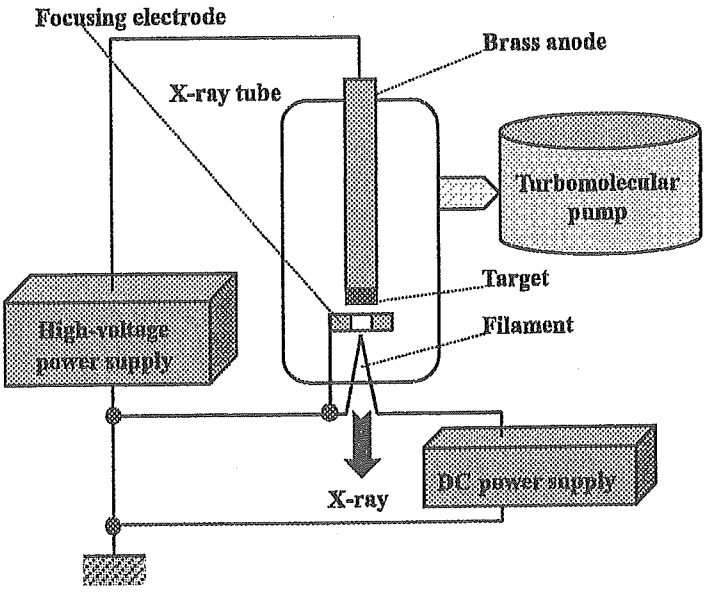

Fig. 1: Block diagram including the main transmission line of the compact x-ray generator with a quasi-monochromatic diode.

forming weakly ionized linear plasma[6-9] using a rod-target triode, we confirmed irradiation of clean K-series characteristic x-rays such as hard x-ray lasers and their higher harmonic hard x-rays from the plasma axial direction. Because the plasma transmits high-photon-energy bremsstrahlung x-rays, it is difficult to produce high-photon-energy characteristic x-rays. In view of this situation, we have developed a super-fluorescent x-ray generator[10-13] by forming weakly ionized plasma at the target tip and have succeeded in producing comparatively clean K-series characteristic x-rays of molybdenum, cerium, tantalum, and tungsten. In particular, the cerium target is useful for performing iodine K-edge angiography, and gadolinium K-edge angiography can be performed using tantalum and tungsten targets.

Steady-state K-series characteristic x-rays left by filters have been employed to perform mammography using a molybdenum target and to perform K-edge angiography[14-17] using a cerium target. In addition, the rays are also useful for performing real-time radiography achieved with a flat panel detector. Because the characteristic x-ray intensity decreases with increases in the filter thickness, the development of a characteristic x-ray generator utilizing the angle dependence of bremsstrahlung x-rays has been wished for.

In the spectrum measurements, we employ a cadmium telluride detector and a lithium fluoride curved crystal. The detector is useful to measure the total spectra including scattering beams. On the other hand, the spectra from only the x-ray source can be measured using the crystal by selecting Bragg's angle.

In this paper, we describe an x-ray generator developed and used to perform a preliminary experiment for generating clean K-series characteristic x-rays by angle dependence of the bremsstrahlung x-rays and measurement of the x-ray spectra using two methods.

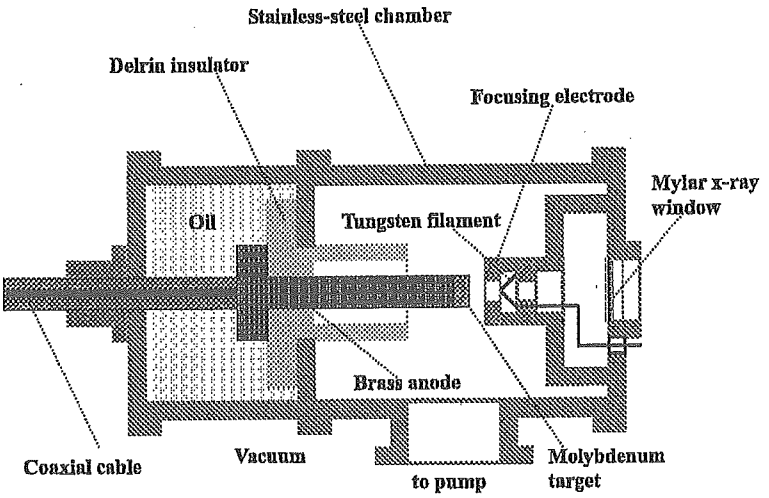

Fig. 2: Schematic drawing of the quasi-monochromatic x-ray tube.

2. Generator

Figure 1 shows a block diagram of a compact characteristic (quasi-monochromatic) x-ray generator. This generator consists of the following components: a constant high-voltage power supply (SL150, Spellman Inc.), a DC filament power supply, a turbomolecular pump, and an x-ray tube. The structure of the x-ray tube is illustrated in Fig. 2. The x-ray tube is a demountable diode which is connected to the turbomolecular pump with a pressure of approximately 0.5 mPa and consists of the following major devices: a molybdenum plate target, a tungsten hairpin cathode (filament), a focusing electrode, a polyethylene terephthalate x-ray window 0.25 mm in thickness, and a stainless-steel tube body. In the x-ray tube, the positive high voltage is applied to the anode (target) electrode, and the cathode is connected to the tube body (ground potential). In this experiment, the tube voltage applied was from 22 to 36 kV, and the tube current was regulated to within 100 μA by the filament temperature. The exposure time is controlled in order to obtain optimum x-ray intensity. The electron beams from the cathode are converged to the target by the focusing electrode, and x-rays are produced through the focusing electrode. Because bremsstrahlung rays are not emitted in the opposite direction to that of electron trajectory, clean molybdenum K-series x-rays can be produced without using a filter.

3. Characteristics

3.1 X-ray intensity

X-ray intensity was measured by a Victoreen 660 ionization chamber at 1.0 m from the x-ray source (Fig. 3). At a constant tube current of 100 μA, the x-ray intensity increased when the tube voltage was

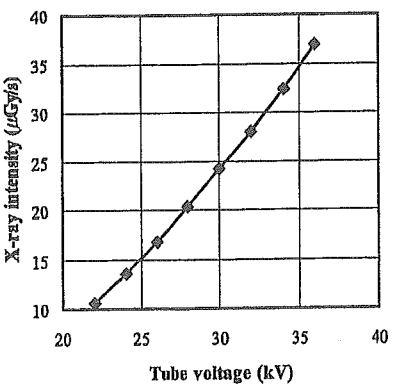

Fig. 3: X-ray intensity at 1.0 m from the x-ray source according to changes in the tube voltage.

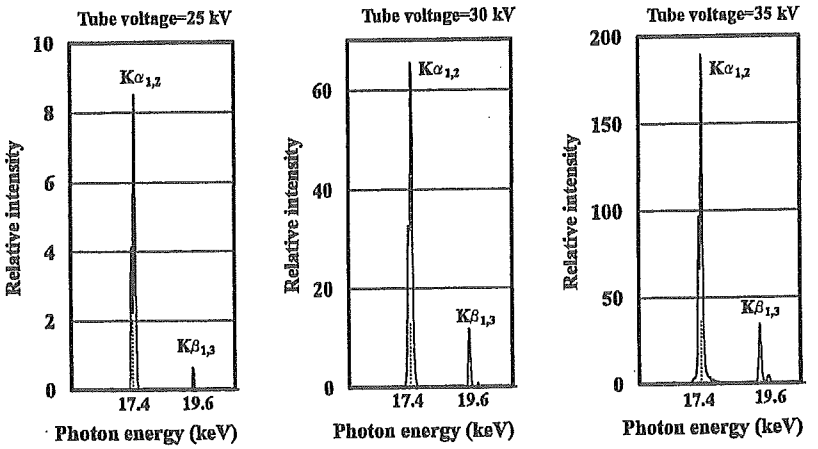

Fig. 4: X-ray spectra from the molybdenum target measured using a transmission type spectrometer with a lithium fluoride curved crystal.

increased. In this measurement, the intensity with a tube voltage of 30 kV and a current of 100 μA was 24.2 μGy/s at 1.0 m from the source.

3.2 X-ray spectra

First, x-ray spectra were measured using a transmission-type spectrometer with a lithium fluoride curved crystal 0.5 mm in thickness. The x-ray intensities of the spectra were detected by an imaging plate of the CR system[18] (Konica Minolta Regius 150) with a wide dynamic range, and relative x-ray intensity was calculated from Dicom original digital data corresponding to x-ray intensity. Figure 4 shows measured spectra from the molybdenum target. We observed clean K lines, while bremsstrahlung

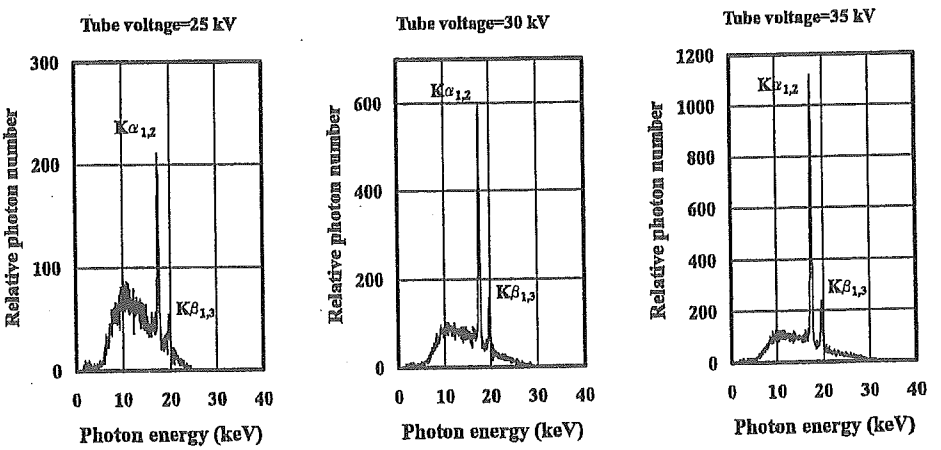

Fig. 5: X-ray spectra from the molybdenum target measured using a cadmium telluride detector.

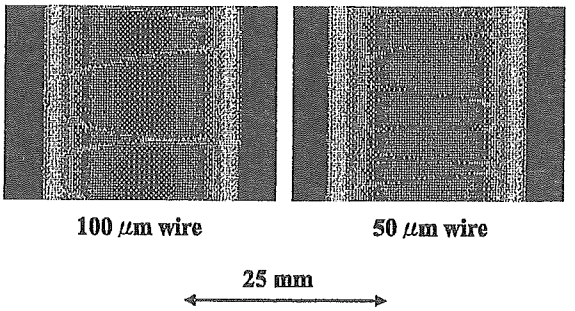

Fig. 6: Radiograms of tungsten wires of 50 and 100 μm in diameter coiled around pipes made of polymethyl methacrylate. A 50-μm-diameter wire could be observed.

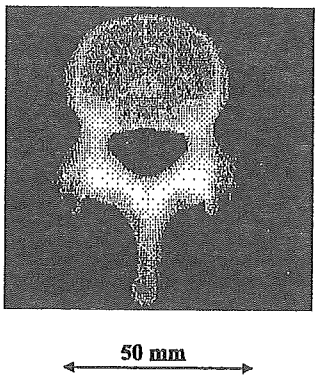

Fig. 7: Radiogram of a vertebra. Fine structure of the vertebra were visible.

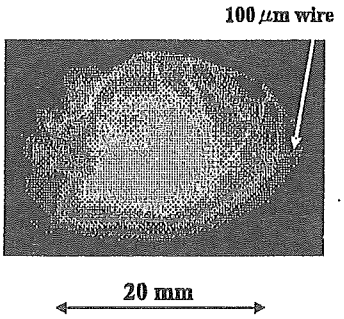

Fig. 8: Angiograms of a rabbit heart. Coronary arteries were visible.

rays were hardly detected. The characteristic x-ray intensity substantially increased with increases in the tube voltage.

The measured spectra using a cadmium telluride detector are shown in Fig. 5. Using the detector, we observed low intensity continuous x-rays. When the tube voltage was increased, both the characteristic x-ray intensity and the maximum photon energy increased.

4. Radiography

The monochromatic radiography was performed by the CR system at 1.0 m from the x-ray source with the filter, and the tube voltage was 30 kV.

First, rough measurements of image resolution were made using wires. Figure 6 shows radiograms of tungsten wires coiled around pipes made of polymethyl methacrylate (PMMA). Although the image contrast increased with increases in the wire diameter, a 50-μm-diameter wire could be observed.

A radiogram of a vertebra is shown in Fig. 7, and the fine structure of the vertebra was observed. Next, angiography was performed using iodine microspheres of 15 μm in diameter. Figure 8 shows an angiogram of a rabbit heart, and we obtained high contrast images of coronary arteries and fine blood vessels.

5. Conclusions and Outlook

In summary, we developed a new characteristic x-ray generator with a molybdenum-target tube and measured clean molybdenum K lines using the crystal spectrometer. However, continuous x-rays were detected using the detector. In both measurements, the characteristic x-ray intensity increased with increases in the tube voltage, and monochromatic Kα lines were left by a zirconium filter. Because we could measure bremsstrahlung x-rays[19] from a transmission-type molybdenum target using the crystal, the bremsstrahlung intensity was low as compared with that obtained using conventional molybdenum tubes.

In this preliminary experiment, although the maximum tube voltage and current were 36 kV and 100 μA, the voltage and current could be increased to 100 kV and 1.0 mA, respectively. Under the pulsed operation, the current can be increased to approximately 1 A without considering the target evaporation. Subsequently, the generator produced maximum number of characteristic photons was approximately 1×10^8 photons/(cm^2 · s) at 1.0 m from the source, and the photon count rate can be increased easily by increasing the current.

Using this x-ray generator, because it is not easy to produce high-photon-energy K-series characteristic x-rays, we are very interested in increasing the energy by changing the electrode configuration between the target, cathode, and focusing electrodes.

Acknowledgments

This work was supported by Grants-in-Aid for Scientific Research (13470154, 13877114, 16591181, and 16591222) and Advanced Medical Scientific Research from MECSST, Health and Labor Sciences Research Grants (RAMT-nano-001, RHGTEFB-genome-005 and RHGTEFB-saisei-003), Grants from the Keiryo Research Foundation, The Promotion and Mutual Aid Corporation for Private Schools of Japan, Japan Science and Technology Agency (JST), and The New Energy and Industrial Technology Development Organization (NEDO, Industrial Technology Research Grant Program in '03).

References

1. R. Germer, "X-ray flash techniques," *J. Phys. E: Sci. Instrum.*, **12**, 336-350, 1979.
2. E. Sato, S. Kimura, S. Kawasaki, H. Isobe, K. Takahashi, Y. Tamakawa and T. Yanagisawa, "Repetitive flash x-ray generator utilizing a simple diode with a new type of energy-selective function," *Rev. Sci. Instrum.*, **61**, 2343-2348, 1990.
3. A. Shikoda, E. Sato, M. Sagae, T. Oizumi, Y. Tamakawa and T. Yanagisawa, "Repetitive flash x-ray generator having a high-durability diode driven by a two-cable-type line pulser," *Rev. Sci. Instrum.*, **65**, 850-856, 1994.
4. E. Sato, K. Takahashi, M. Sagae, S. Kimura, T. Oizumi, Y. Hayasi, Y. Tamakawa and T. Yanagisawa, "Sub-kilohertz flash x-ray generator utilizing a glass-enclosed cold-cathode triode," *Med. & Biol. Eng. & Comput.*, **32**, 289-294, 1994.
5. K. Takahashi, E. Sato, M. Sagae, T. Oizumi, Y. Tamakawa and T. Yanagisawa, "Fundamental study on a long-duration flash x-ray generator with a surface-discharge triode," *Jpn. J. Appl. Phys.*, **33**, pp. 4146-4151, 1994.
6. E. Sato, Y. Hayasi, R. Germer, E. Tanaka, H. Mori, T. Kawai, T. Ichimaru, K. Takayama and H. Ido,

"Quasi-monochromatic flash x-ray generator utilizing weakly ionized linear copper plasma," *Rev. Sci. Instrum.*, **74**, 5236-5240, 2003.

7. E. Sato, Y. Hayasi, R. Germer, E. Tanaka, H. Mori, T. Kawai, H. Obara, T. Ichimaru, K. Takayama and H. Ido, "Irradiation of intense characteristic x-rays from weakly ionized linear molybdenum plasma," *Jpn. J. Med. Phys.*, **23**, 123-131, 2003.
8. E. Sato, Y. Hayasi, R. Germer, E. Tanaka, H. Mori, T. Kawai, T. Ichimaru, S. Sato, K. Takayama and H. Ido, "Sharp characteristic x-ray irradiation from weakly ionized linear plasma," *J. Electron Spectrosc. Related Phenom.*, **137-140**, 713-720, 2004.
9. E. Sato, E. Tanaka, H. Mori, T. Kawai, S. Sato and K. Takayama, "Clean monochromatic x-ray irradiation from weakly ionized linear copper plasma," *Opt. Eng.*, **44**, 049002-1-6, 2005.
10. E. Sato, M. Sagae, E. Tanaka, Y. Hayasi, R. Germer, H. Mori, T. Kawai, T. Ichimaru, S. Sato, K. Takayama and H. Ido, "Quasi-monochromatic flash x-ray generator utilizing a disk-cathode molybdenum tube," *Jpn. J. Appl. Phys.*, **43**, 7324-7328, 2004.
11. E. Sato, E. Tanaka, H. Mori, T. Kawai, T. Ichimaru, S. Sato, K. Takayama and H. Ido, "Compact monochromatic flash x-ray generator utilizing a disk-cathode molybdenum tube," *Med. Phys.*, **32**, 49-54, 2005.
12. E. Sato, E. Tanaka, H. Mori, T. Kawai, T. Inoue, A. Ogawa, S. Sato, K. Takayama and H. Ido, "High-speed K-edge angiography achieved with tantalum K-series characteristic x rays," *SPIE*, **5745**, 810-817, 2005.
13. E. Sato, Y. Hayasi, R. Germer, K. Kimura, E. Tanaka, H. Mori, T. Kawai, T. Inoue, A. Ogawa, S. Sato, K. Takayama and H. Ido, "Enhanced K-edge plasma angiography achieved with tungsten Kα rays utilizing gadolinium-based contrast media," *SPIE*, **5920**, 592012-1-8, 2005.
14. E. Sato, Y. Hayasi, R. Germer, E. Tanaka, H. Mori, T. Kawai, T. Ichimaru, S. Sato, K. Takayama and H. Ido, "Portable x-ray generator utilizing a cerium-target radiation tube for angiography," *J. Electron Spectrosc. Related Phenom.*, **137-140**, 699-704, 2004.
15. E. Sato, E. Tanaka, H. Mori, T. Kawai, T. Ichimaru, S. Sato, K. Takayama and H. Ido, "Demonstration of enhanced K-edge angiography using a cerium target x-ray generator," *Med. Phys*, **31**, 3017-3021, 2004.
16. E. Sato, R. Germer, E. Tanaka, H. Mori, T. Kawai, T. Ichimaru, S. Sato, H. Ojima, K. Takayama and H. Ido, "Quasi-monochromatic cerium flash angiography," *SPIE*, **5580**, 146-152, 2005.
17. E. Sato, E. Tanaka, H. Mori, T. Kawai, T. Inoue, A. Ogawa, A. Yamadera, S. Sato. F. Ito, K. Takayama and H. Ido, "Variations in cerium x-ray spectra and enhanced K-edge angiography," *Jpn. J. Appl. Phys*, **44**, 8204-8209, 2005.
18. E. Sato, K. Satoi and Y. Tamakawa, "Film-less computed radiography system for high-speed imaging," *Ann. Rep. Iwate Med. Univ. Sch. Lib. Arts and Sci.*, **35**, 13-23, 2000.
19. M. Sagae, E. Sato, E. Tanaka, Y. Hayasi, R. Germer, H. Mori, T. Kawai, T. Ichimaru, S. Sato, K. Takayama and H. Ido, "Quasi-monochromatic x-ray generator utilizing graphite cathode diode with transmission-type molybdenum target," *Jpn. J. Appl. Phys.*, **44**, 446-449, 2005.

Annual Report of Iwate Medical University
School of Liberal Arts and Sciences
No. 40 (2005), 9-15.

Measurement of Cerium X-ray Spectra Using a Cerium Oxide Powder Filter and Enhanced K-edge Angiography

Eiichi Sato[a], Etsuro Tanaka[b], Hidezo Mori[c], Toshiaki Kawai[d], Takashi Inoue[e], Akira Ogawa[e], Kiyomi Takahashi[f], Shigehiro Sato[f] and Kazuyoshi Takayama[g]

(Received October 31, 2005)

Abstract

The cerium-target x-ray tube is useful in order to perform cone-beam K-edge angiography because K-series characteristic x-rays from the cerium target are absorbed effectively by iodine-based contrast media. The x-ray generator consists of a main controller and a unit with a high-voltage circuit and a fixed anode x-ray tube. The tube is a glass-enclosed diode with a cerium target and a 0.5-mm-thick beryllium window. The maximum tube voltage and current were 70 kV and 0.40 mA, respectively, and the focal-spot sizes were approximately 1×1 mm. Cerium K-series characteristic x-rays were left using a cerium oxide powder filter, and the x-ray intensity was 14.3 μGy/s at 1.0 m from the source with a tube voltage of 60 kV, a current of 0.40 mA, and an exposure time of 1.0 s. Angiography was performed with a computed radiography system using iodine-based microspheres 15 μm in diameter. In angiography of non-living animals, we observed fine blood vessels of approximately 100 μm with high contrasts.

Keywords: x-ray tube, cerium target, cerium oxide filter, powder filter, characteristic x-rays, K-edge angiography

1. Introduction

Flash x-ray generators are useful for performing high-speed radiography,[1] and several different generators with maximum photon energies of 150 keV[2-6] have been applied to biomedical radiography. By forming weakly ionized linear plasma[6-9] using a cold-cathode triode, we have succeeded in producing K-series characteristic x-rays of nickel and copper. Subsequently, we have developed super-fluorescent

[a] Department of Physics, Iwate Medical University, 3-16-1 Honchodori, Morioka 020-0015, Japan
[b] Department of Nutritional Science, Faculty of Applied Bio-science, Tokyo University of Agriculture, 1-1-1 Sakuragaoka, Setagaya-ku 156-8502, Japan
[c] Department of Cardiac Physiology, National Cardiovascular Center Research Institute, 5-7-1 Fujishirodai, Suita, Osaka 565-8565, Japan
[d] Electron Tube Division #2, Hamamatsu Photonics K. K., 314-5 Shimokanzo, Iwata 438-0193, Japan
[e] Department of Neurosurgery, School of Medicine, Iwate Medical University, 19-1 Uchimaru, Morioka 020-8505, Japan
[f] Department of Microbiology, School of Medicine, Iwate Medical University, 19-1 Uchimaru, Morioka 020-8505, Japan
[g] Shock Wave Research Center, Institute of Fluid Science, Tohoku University, 2-1-1 Katahira, Sendai 980-8577, Japan

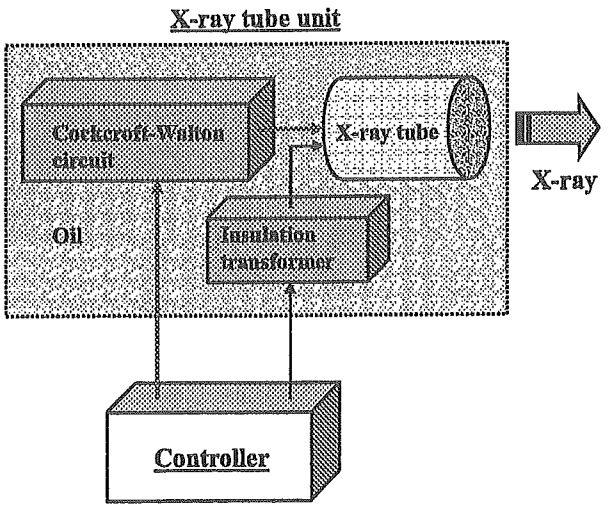

Fig. 1: Block diagram of the compact x-ray generator with a cerium-target radiation tube, which is used specially for K-edge angiography using iodine-based contrast media.

x-ray generator[10-13] to produce comparatively clean high-photon-energy characteristic x-rays of cerium and tungsten.

To produce steady state x-rays, synchrotrons generate high-dose-rate bremsstrahlung x-rays, and monochromatic parallel beams are formed using single crystals. In particular, x-rays of approximately 35 keV have been applied to perform enhanced K-edge angiography[14,15] and phase-contrast radiography,[16,17] including dark-field imaging using an analyzer crystal. Using these imaging, although the spatial resolution has been improved, it is difficult to increase the irradiation field due to the parallelity. Recently, we have developed a steady-state x-ray generator utilizing a cerium-target tube[18-20] and have demonstrated enhanced K-edge angiography utilizing a barium sulfate filter. In this research, Kα lines (34.6 keV) were left by absorbing Kβ lines (39.2 keV), and bremsstrahlung x-rays with photon energies lower than the barium K-edge (37.4 keV) were also observed. However, because cerium Kβ lines are also absorbed effectively by iodine, both Kα and Kβ lines should be selected to perform angiography.

In the present research, we measured the x-ray spectra from a cerium-target tube using a new cadmium telluride detector, and performed a preliminary study on cone-beam K-edge angiography achieved with cerium characteristic x-rays using a cerium oxide powder filter.

2. Generator

Figure 1 shows the block diagram of the x-ray generator, which consists of a main controller and an x-ray tube unit with a Cockcroft-Walton circuit and a cerium-target tube. The tube voltage, the current, and the exposure time can be controlled by the controller. The main circuit for producing x-rays is illustrated in Fig. 2, and employed the Cockcroft-Walton circuit in order to decrease the dimensions of the tube unit. In the x-ray tube, the negative high-voltage is applied to the cathode electrode, and the anode (target) is connected to the tube unit case (ground potential) to cool the anode and the target effectively. The filament heating current is supplied by an AC power supply in the controller in

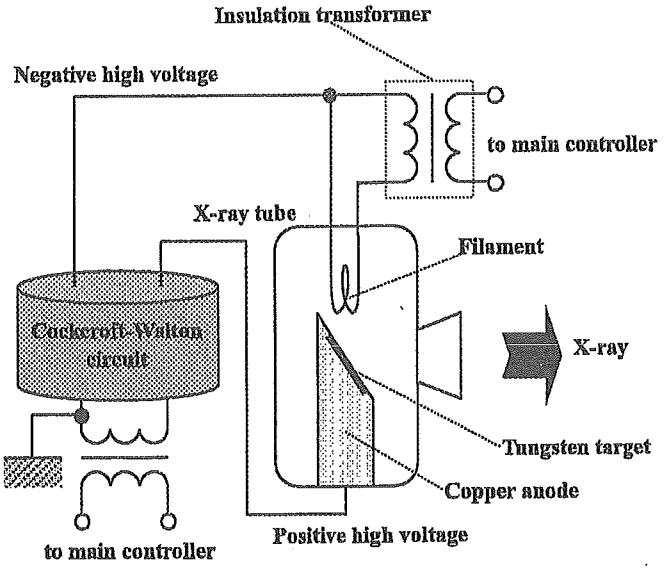

Fig. 2: Main circuit of the x-ray generator.

conjunction with an insulation transformer. In this experiment, the tube voltage applied was from 45 to 70 kV, and the tube current was regulated to within 0.40 mA (maximum current) by the filament temperature. The exposure time is controlled in order to obtain optimum x-ray intensity. Quasi-monochromatic x-rays are produced using a cerium oxide power filter with a surface density of 30 mg/cm^2.

3. Characteristics

3.1 X-ray Intensity

X-ray intensity was measured by a Victoreen 660 ionization chamber at 1.0 m from the x-ray source using the filter with an exposure time of 1.0 s (Fig. 3). At a constant tube current of 0.40 mA, the x-ray intensity increased when the tube voltage was increased. In this measurement, the intensity with a tube voltage of 60 kV and a current of 0.40 mA was 14.3 μGy/s at 1.0 m from the source.

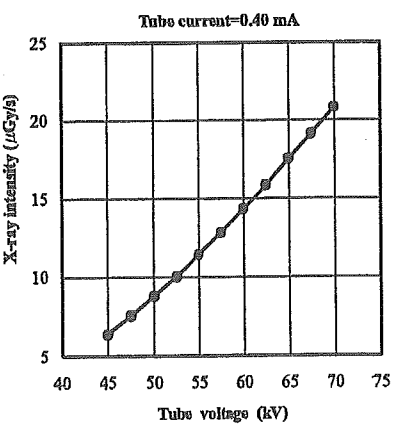

Fig. 3: X-ray intensity measured at 1.0 m from the x-ray source according to changes in the tube voltage.

3.2 Focal spot

In order to measure images of the x-ray source after the filtration, we employed a pinhole camera with a hole diameter of 50 μm (magnification ratio of 1:2) in conjunction with a Computed Radiography (CR)

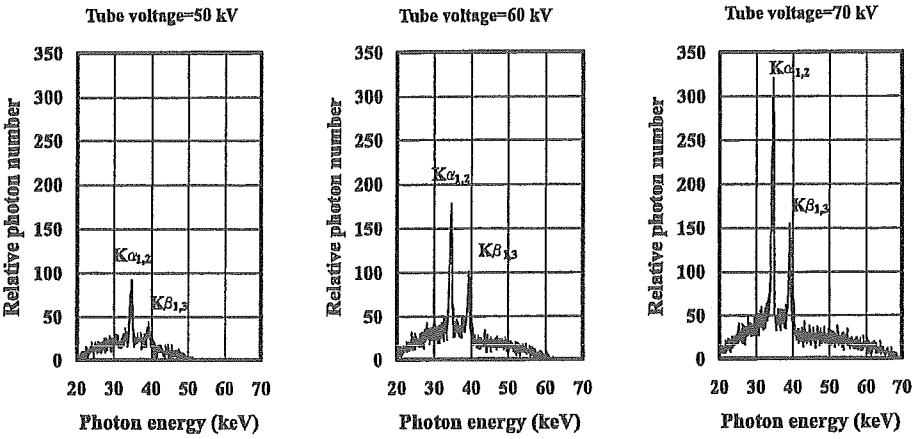

Fig. 4: X-ray spectra measured using a cadmium telluride detector with changes in the tube voltage.

system[21] with a sampling pitch of 87.5 μm. When the tube voltage was increased, spot dimensions increased slightly and had values of approximately 1×1 mm.

3.3 X-ray spectra

In order to measure x-ray spectra, we employed a cadmium telluride detector (XR-100T, Amptek Inc.) (Fig. 4). When the tube voltage was increased, the characteristic x-ray intensities of Kα and Kβ lines substantially increased, and both the maximum photon energy and the intensities of bremsstrahlung x-rays increased.

4. K-edge Angiography

Cerium is a rare earth element and has a high reactivity; however, the average photon energies of Kα and Kβ lines are 34.6 and 39.2 keV, respectively, and iodine contrast media with a K-absorption edge of

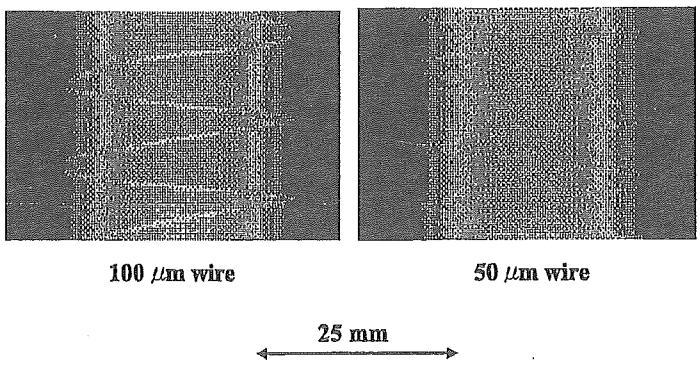

Fig. 5: Radiograms of tungsten wires coiled around PMMA rods.

33.2 keV absorb the lines easily. Therefore, blood vessels were observed with high contrasts.

The angiography was performed by the CR system[21] (Konica Regius 150) using the filter with a tube voltage of 60 kV, and the distance (between the x-ray source and the imaging plate) was 1.5 m. First, rough measurements of spatial resolution were made using wires. Figure 5 shows radiograms of tungsten wires coiled around rods made of polymethyl methacrylate. Although the image contrast decreased somewhat with decreases in the wire diameter, due to blurring of the image caused by the sampling pitch of 87.5 μm, a 50-μm-diameter wire could be observed.

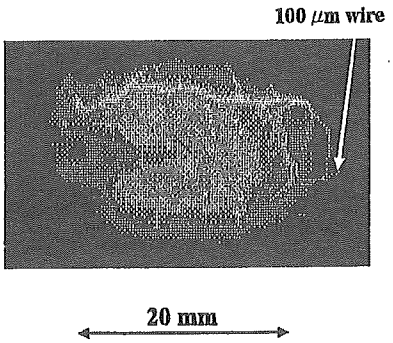

Fig. 6: Angiograms of an extracted rabbit heart using iodine microspheres.

An angiograms of a rabbit heart is shown in Fig. 6. This image was obtained using iodine microspheres of 15 μm in diameter. Fine blood vessels in the coronary arteries in the heart were visible. Figure 7 shows an angiogram of a larger dog heart using iodine spheres, and blood vessels of approximately 100 μm in diameter were visible.

5. Discussion

In summary, we employed an x-ray generator with a cerium-target tube and succeeded in producing cerium K-series characteristic x-rays, which can be absorbed easily by iodine-based contrast media. In the spectrum measurement, high-photon-energy bremsstrahlung x-rays beyond cerium K-edge (40.4 keV) were absorbed effectively.

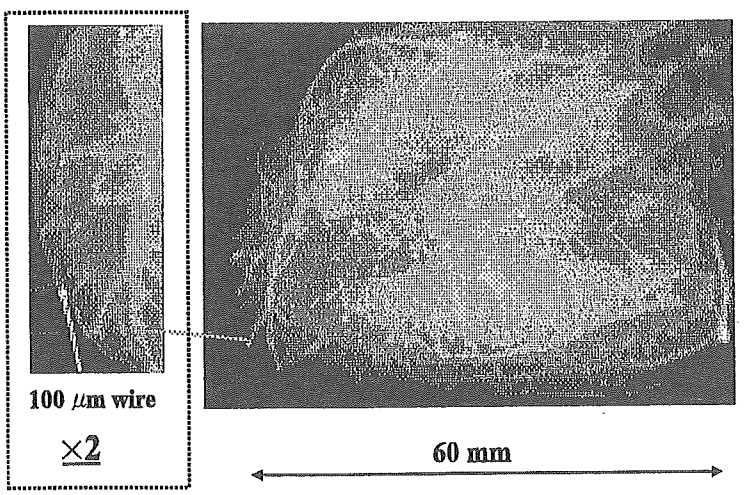

Fig. 7: Angiograms of an extracted dog heart using iodine microspheres.

In angiography, fine blood vessels were observed with high contrast with a spatial resolution of approximately 100 μm; the resolution was almost equal to the sampling pitch (87.5 mm) of the CR system. Therefore, the pith should be minimized, and magnification digital radiography including phase-contrast effect should be employed in order to improve the spatial resolution.

Although the cerium x-ray generator used in this research produces both the characteristic and the bremsstrahlung x-rays, bremsstrahlung intensity can be decreased effectively by considering the angle dependence without using the filter, since bremsstrahlung rays are not emitted in the opposite direction to that of electron trajectory. Subsequently, the generator produced maximum number of estimated characteristic photons was approximately 5×10^7 photons / ($cm^2 \cdot s$) at 1.0 m from the source, and the photon count rate can be increased easily by improving the target.

Acknowledgment

This work was supported by Grants-in-Aid for Scientific Research (13470154, 13877114, 16591181, and 16591222) and Advanced Medical Scientific Research from MECSST, Health and Labor Sciences Research Grants (RAMT-nano-001, RHGTEFB-genome-005 and RHGTEFB-saisei-003), Grants from the Keiryo Research Foundation, The Promotion and Mutual Aid Corporation for Private Schools of Japan, Japan Science and Technology Agency (JST), and The New Energy and Industrial Technology Development Organization (NEDO, Industrial Technology Research Grant Program in '03).

References

1. R. Germer, "X-ray flash techniques," *J. Phys. E: Sci. Instrum.*, **12**, 336-350, 1979.
2. E. Sato, S. Kimura, S. Kawasaki, H. Isobe, K. Takahashi, Y. Tamakawa and T. Yanagisawa, "Repetitive flash x-ray generator utilizing a simple diode with a new type of energy-selective function," *Rev. Sci. Instrum.*, **61**, 2343-2348, 1990.
3. A. Shikoda, E. Sato, M. Sagae, T. Oizumi, Y. Tamakawa and T. Yanagisawa, "Repetitive flash x-ray generator having a high-durability diode driven by a two-cable-type line pulser," *Rev. Sci. Instrum.*, **65**, 850-856, 1994.
4. E. Sato, K. Takahashi, M. Sagae, S. Kimura, T. Oizumi, Y. Hayasi, Y. Tamakawa and T. Yanagisawa, "Sub-kilohertz flash x-ray generator utilizing a glass-enclosed cold-cathode triode," *Med. & Biol. Eng. & Comput.*, **32**, 289-294, 1994.
5. K. Takahashi, E. Sato, M. Sagae, T. Oizumi, Y. Tamakawa and T. Yanagisawa, "Fundamental study on a long-duration flash x-ray generator with a surface-discharge triode," *Jpn. J. Appl. Phys.*, **33**, pp. 4146-4151, 1994.
6. E. Sato, Y. Hayasi, R. Germer, E. Tanaka, H. Mori, T. Kawai, T. Ichimaru, K. Takayama and H. Ido, "Quasi-monochromatic flash x-ray generator utilizing weakly ionized linear copper plasma," *Rev. Sci. Instrum.*, **74**, 5236-5240, 2003.
7. E. Sato, Y. Hayasi, R. Germer, E. Tanaka, H. Mori, T. Kawai, H. Obara, T. Ichimaru, K. Takayama and H. Ido, "Irradiation of intense characteristic x-rays from weakly ionized linear molybdenum plasma," Jpn. J. Med. Phys., 23, 123-131, 2003.
8. E. Sato, Y. Hayasi, R. Germer, E. Tanaka, H. Mori, T. Kawai, T. Ichimaru, S. Sato, K. Takayama and H. Ido, "Sharp characteristic x-ray irradiation from weakly ionized linear plasma," *J. Electron*